Macromolecules

pubs.acs.org/Macromolecules Article

Crown Ether-Functionalized Polybenzoxazine for Metal Ion Adsorption

Mohamed Gamal Mohamed and Shiao-Wei Kuo*

Cite This: *Macromolecules* 2020, 53, 2420−2429 Read Online

ACCESS | Metrics & More | Article Recommendations | Supporting Information

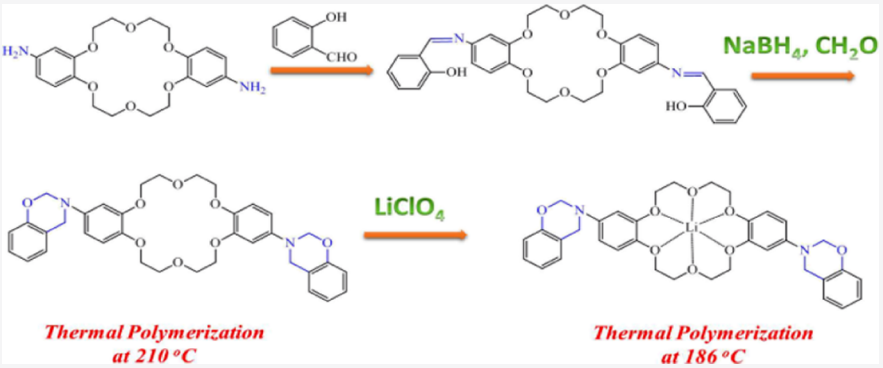

ABSTRACT: In this study, we synthesized a new crown ether-functionalized benzoxazine monomer (crown-ether BZ) in high yield and purity through reduction of the Schiff base prepared from a dibenzo[18]crown-6 diamine derivative and salicylaldehyde and subsequent reaction of the resulting *o*-hydroxybenzylamine species with CH_2O. We used differential scanning calorimetry (DSC), Fourier transform infrared (FTIR) spectroscopy, and thermogravimetric analysis to examine the thermal ring opening polymerization and thermal stability of the crown-ether BZ monomer during various types of thermal treatment. DSC revealed that this crown-ether BZ monomer featured a relatively low curing temperature (210 °C; that of the typical Pa-type 3-phenyl-3,4-dihydro-2*H*-benzooxazine monomer: 263 °C) because the flexibility of the crown ether moiety on the main chain backbone structure catalyzed the ring opening polymerization. We also used DSC, FTIR spectroscopy, and ionic conductivity measurements to investigate the specific metal−crown ether interactions of crown-ether BZ/$LiClO_4$ complexes. The presence of Li^+ ions decreased the curing temperature significantly to 186 °C, suggesting that the metal ions functioned as an effective catalyst and promoter that accelerated the ring opening polymerization of the crown-ether BZ monomer. The ionic conductivity reached 8.3×10^{-5} S cm^{-1} for the crown-ether BZ/$LiClO_4$ = 90/10 complex after thermal curing; this value is higher than those of typical polymer-based systems (e.g., PEO, PCL, PMMA, and PVP) while also providing a polymer electrolyte of higher thermal stability.

INTRODUCTION

Polybenzoxazine (PBZ) is a new type of thermosetting resin that has the potential to replace traditional phenolic, epoxy, and bismaleimide resins.[1−4] PBZs can be obtained as highly cross-linked network materials through thermal ring opening polymerization of benzoxazine monomers, which are themselves prepared through Mannich condensations of primary/aromatic amines, phenolic derivatives, and paraformaldehyde.[5−10] Because of intra- and intermolecular hydrogen bonding between their phenolic and tertiary amino groups after ring opening polymerization of the benzoxazine unit in their Mannich bridges, PBZ materials are attracting the attention of academia and industry for their unique characteristics, including catalyst-free polymerization; low outgassing and shrinkage upon curing; low surface free energies; excellent mechanical, electrical, and chemical resistance; high char yields; low dielectric constants; ease of processability; good flame retardancy; no liberation of byproducts; low water absorption; and high thermal stability.[11−21] Furthermore, the properties of these thermosetting resins can be tailored by varying their structures through molecular design flexibility (e.g., the introduction of nitrile, hydroxyalkyl, alkyl, carboxyl, or propargyl groups)[22−32] or the incorporation of inorganic materials [e.g., polydimethylsiloxane, nanoclay, polyhedral oligomeric silsesquioxane, carbon nanotubes, or graphene] into the benzoxazine matrix.[7,8,33−45]

Crown ethers are excellent complexing agents that are capable of capturing metal cations within their cavities.[46] They

Received: November 28, 2019
Revised: January 18, 2020
Published: March 18, 2020

https://dx.doi.org/10.1021/acs.macromol.9b02519
Macromolecules 2020, 53, 2420−2429

Scheme 1. Synthesis of Crown-Ether BZ (h) from (a) Catechol, (b) Dibenzo[18]crown-6, (c) Dibenzo-crownether-2NO_2, (d) Dibenzo-crownether-2NH_2, (f) Dibenzo-crownether-salicylaldehyde, and (g) Dibenzo-crownether-hydroxybenzylamine

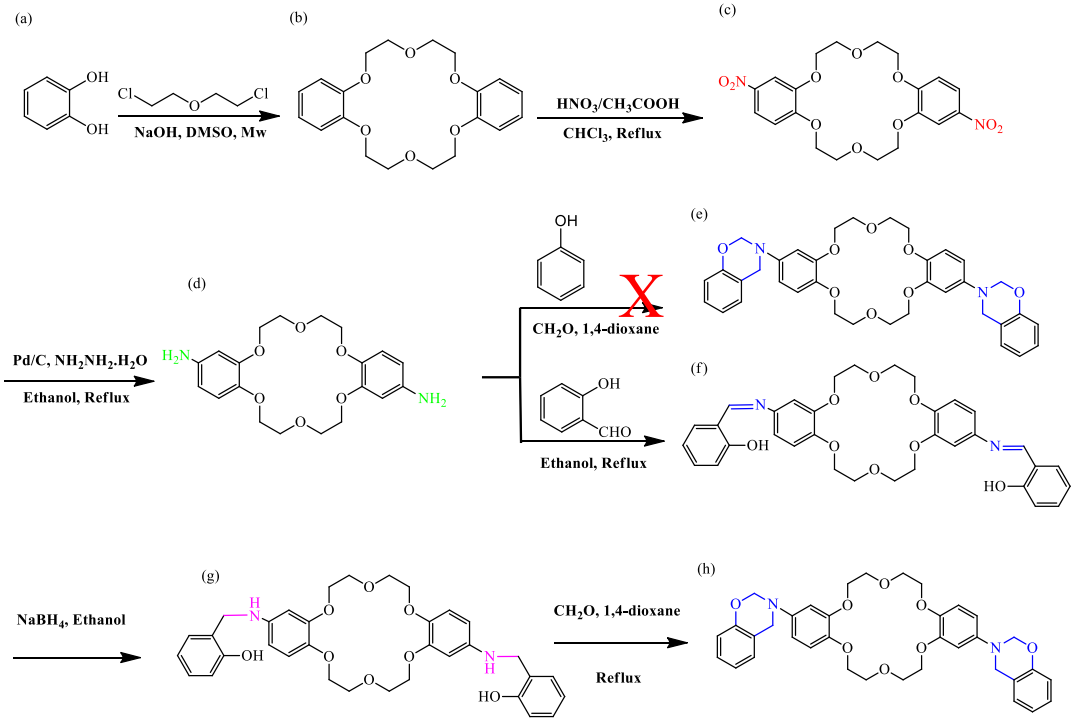

are attractive materials for application in various biological systems because they can form complex systems with various metal cations, in a process that is strongly dependent on the size of the crown ether ring and the diameter of the metal cation.[47] Many crown ether-functionalized polymers have been synthesized and generally connected with reactive materials or metal ion channels.[48,49] Crown ether-functionalized polymers can extract alkali metal cations from aqueous solutions through solvent extraction, with potential application in the treatment of wastewater.[49] For this study, we wished to exploit the properties of PBZs and crown ethers to synthesize a new crown ether-functionalized PBZ.[50]

Here, we prepared a new benzoxazine monomer (crown-ether BZ), containing dibenzo[18]crown-6-functionalized units, through reduction of the Schiff base obtained from di(aminobenzo)[18]crown-6 (dibenzo-crownether-2NH_2) and salicylaldehyde and subsequent treatment of the *o*-hydroxybenzylamine derivative with paraformaldehyde in 1,4-dioxane and absolute EtOH at 100 °C for 12 h (Scheme 1). Fourier transform infrared (FTIR) spectroscopy, nuclear magnetic resonance (NMR) spectroscopy, and high-resolution mass spectrometry confirmed the chemical structure of crown-ether BZ. We used differential scanning calorimetry (DSC), thermogravimetric analysis (TGA), and FTIR spectroscopy to investigate the thermal ring-opening polymerization behavior and thermal stability of crown-ether BZ before and after ring opening polymerization of its oxazine moiety. Furthermore, we employed DSC, FTIR spectroscopy, and ionic conductivity measurements to investigate the specific metal-crown ether interactions of crown-ether BZ blended with lithium perchlorate ($LiClO_4$) at various weight ratios, before and after ring opening polymerization.

EXPERIMENTAL SECTION

Materials. Catechol (98%), dichloromethane (CH_2Cl_2), hydrazine monohydrate ($NH_2NH_2{\cdot}H_2O$), *N*,*N*-dimethylacetamide (DMAc), dimethyl sulfoxide (DMSO), absolute EtOH (C_2H_5OH, 99.99%), MeOH (CH_3OH), xylene, chlorobenzene, dimethylformamide (DMF), toluene, anhydrous magnesium sulfate ($MgSO_4$), acetic acid, chloroform ($CHCl_3$), $LiClO_4$, bis(2-chloroethyl) ether, and sodium hydroxide (NaOH) were purchased from Sigma-Aldrich. Palladium activated on carbon (Pd/C, 10 wt %), 1,4-dioxane, paraformaldehyde $(CH_2O)_n$, nitric acid (HNO_3, 65%), hydrochloric acid (HCl, 37%), and acetone were purchased from Acros. Dibenzo[18]crown-6, *trans*-di(nitrobenzo)[18]crown-6 (dibenzo-crownether-2NO_2), and *trans*-di(aminobenzo)[18]crown-6 (dibenzo-crownether-2NH_2) were synthesized according to previously a literature method with minor modification[51] [Figures S1−S5].

***N*,*N*′-Bis(salicylidene)-4,4′-diimino-2.3.11,12-dibenzo-1,4,7,10,13,l6-16-hexaoxacyclooctadeca-2,11-diene (Dibenzo-crownether-salicylaldehyde).** A solution of dibenzo-crownether-2NH_2 (2.00 g, 5.13 mmol) and salicylaldehyde (1.07 mL, 10.3 mmol) in absolute EtOH (100 mL) was heated under reflux at 80 °C for 4 h in a 250 mL flask equipped with a reflux condenser. After cooling, the yellow solid was filtered off, washed three times with EtOH, and dried under vacuum at 50 °C for 24 h to give the title compound (1.85 g, 92%). FTIR (KBr, cm^{-1}): 3446 (O−H stretching), 3064 (aromatic C−H stretching), 1620 (C−N stretching). ^{1}H NMR (DMSO-d_6, 25 °C, 500 MHz): δ 13.34 (s, 2H, OH), 8.96 (s, 2H), 7.61−6.93 (m, ArH), 4.06−3.87 (m, 8H), 3.86−3.71 (m, 8H). ^{13}C NMR (DMSO-d_6, 25 °C, 125 MHz): δ 161.28, 160.21, 148.52, 147.39, 140.768, 132.78, 132.35, 119.41, 116.56, 113.97, 112.41, 68.85, 67.86.

***N*,*N*′-Bis(salicylidene)-4,4′-diamino-2.3.11,12-dibenzo-1,4,7,10,13,l6-16 Hexaoxacycloocta Decane (Dibenzo-crownether-hydroxybenzylamine).** A mixture of dibenzo-crownether-salicylaldehyde (1.00 g, 1.70 mmol), $NaBH_4$ (0.254 g, 6.68 mmol), and DMAc (10 mL) in a 50 mL two-neck flask was stirred at room temperature for 24 h. The mixture was then poured into ice-water (300 mL). The white solid obtained after filtration was washed three times with water to give a white solid (0.90 g, 90%). FTIR (KBr, cm^{-1}): 3353 (O−H stretching), 3280 (N−H stretching), 2939

https://dx.doi.org/10.1021/acs.macromol.9b02519
Macromolecules 2020, 53, 2420−2429

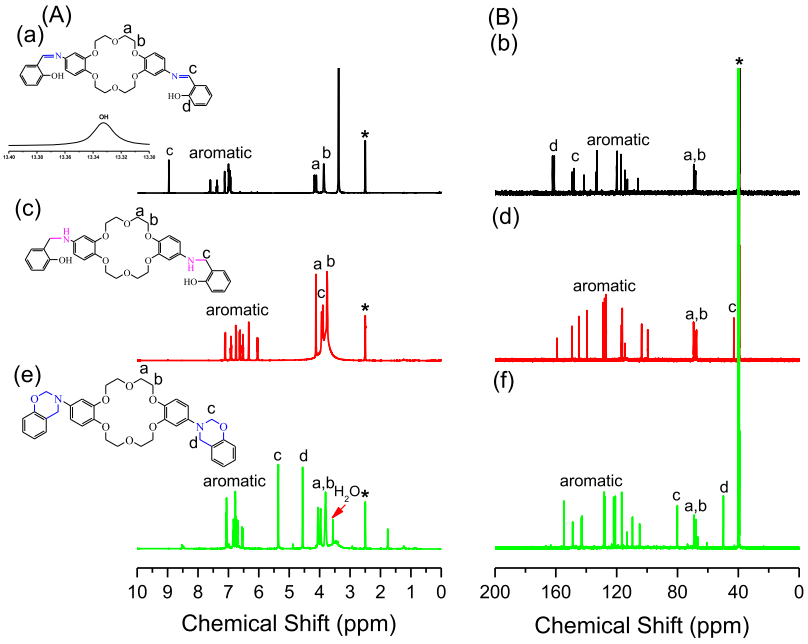

Figure 1. (A) ^{1}H and (B) ^{13}C NMR spectra of (a,d) dibenzo-crownether-salicylaldehyde, (b,e) dibenzo-crownether-hydroxybenzylamine, and (c,f) crown-ether BZ in DMSO-d_6.

(aliphatic C−H stretching). ^{1}H NMR (DMSO-d_6, 25 °C, 500 MHz): δ 7.11−6.03 (m, ArH), 4.17 (s, 4H), 4.06−3.87 (m, 8H), 3.86−3.71 (m, 8H).^{13}C NMR (DMSO-d_6, 25 °C, 125 MHz): δ 158.42, 148.56, 138.86, 128.25, 127.31, 126.33, 116.28, 115.71, 113.99, 103.06, 99.03, 68.85, 67.86, 42.69.

Crown-Ether BZ. A solution of dibenzo-crownether-hydroxybenzylamine (1.00 g, 1.70 mmol) and paraformaldehyde (0.100 g, 3.33 mmol) in 1,4-dioxane (40 mL) and absolute EtOH (20 mL) in a 100 mL two-neck flask was heated at 100 °C for 10 h under a N_2 atmosphere. After evaporating the solvents, the brown residue was dissolved in EtOAc (100 mL). The solution was washed with 1 N $NaHCO_3$. The organic phase was concentrated under reduced pressure to obtain a white solid (0.85 g, 85%). FTIR (KBr, cm^{-1}): 1360 (tetrasubstituted benzene ring), 1240 (asymmetric C−O−C stretching), 1044 (symmetric C−O−C stretching), 937 (oxazine ring). ^{1}H NMR (DMSO-d_6, 25 °C, 500 MHz): δ 7.08−6.53 (m, ArH), 5.36 (s, OCH_2N), 4.56 (s, NCH_2Ar), 4.06−3.87 (m, 8H), 3.86−3.71 (m, 8H). ^{13}C NMR (DMSO-d_6, 25 °C, 125 MHz): δ 153.89, 148.21, 142.43, 127.55, 121.30, 120.28, 116.06, 112.66, 109.07, 104.37, 79.67, 68.84, 67.74, 49.56. High resolution FT-MS: calcd for $C_{36}H_{38}N_2O_8$, m/z 626.26; found, 649.26 $[M + Na]^+$ (Figure S6).

Crown Ether-Functionalized PBZ. Crown-ether BZ was thermally activated cured in a stepwise manner at various temperatures (110, 150, 180, and 210 °C) for 2 h at each temperature to provide a dark brown solid.

Crown Ether-Functionalized PBZ/$LiClO_4$ Complexes. Various amounts of $LiClO_4$ were dissolved in DMF (5 mL). A solution of $LiClO_4$ was added dropwise to a solution of crown-ether BZ in DMF (5 mL). The solutions of the crown-ether BZ/$LiClO_4$ complexes were stirred at 50 °C for 48 h. The evaporation of the DMF was under reduced pressure, each blend mixture was thermally activated cured at 110, 150, 180, and 210 °C (2 h at each temperature).

RESULTS AND DISCUSSION

Synthesis of Dibenzo-Crownether-2NH_2. Scheme 1 presents our method for the synthesis of the crown ether-functionalized benzoxazine monomer. First, we prepared dibenzo[18]crown-6 as fibrous white needles of high purity through the reaction of catechol [Scheme 1a] with bis(2-chloroethyl) ether in the presence NaOH [Scheme 1b]. Nitration of dibenzo[18]crown-6 in the presence 65% HNO_3 and acetic acid in $CHCl_3$ for 3 h afforded dibenzo-crownether-2NO_2 as a white powder [Scheme 1(c)]. Reduction of dibenzo-crownether-2NO_2 with hydrazine monohydrate in the presence of 10 wt % Pd/C in absolute EtOH and 1,4-dioxane as co-solvents at 90 °C for 48 h provided dibenzo-crownether-2NH_2 as a white powder of high purity and in high yield [Scheme 1d].[51] We employed NMR and FTIR spectroscopy to confirm the chemical structures of our synthesized compounds.

Figure S4A displays ^{1}H NMR spectra, recorded at room temperature, of dibenzo[18]crown-6, dibenzo-crownether-2NO_2, and dibenzo-crownether-2NH_2 in DMSO-d_6. The characteristic signals for the aromatic protons and O-methylene protons of dibenzo[18]crown-6 [Figure S4A-a] appeared at 6.94−6.85 and 4.06−3.83 ppm, respectively. The ^{1}H NMR spectrum [Figure S4A-b] of dibenzo-crownether-2NO_2 featured signals at 7.09−7.17 ppm for the aromatic protons and 4.23−3.84 ppm for the aliphatic protons of the crown ether unit. Figure S4A-c reveals that the signals for the aromatic protons of dibenzo-crownether-2NH_2 shifted to 6.63−6.23 ppm after reduction of dibenzo-crownether-2NO_2. Furthermore, the characteristic signal of the NH protons appeared at 4.63 ppm, whereas the signals of the O-methylene protons of the crown ether moiety appeared at 3.96−3.76 ppm. Figure S4B presents ^{13}C NMR spectra, recorded at room temperature, of dibenzo[18]crown-6, dibenzo-crownether-2NO_2, and dibenzo-crownether-2NH_2 in DMSO-d_6. The signals for the aromatic and O-methylene carbon nuclei of dibenzo[18]crown-6 appeared at 147.96, 120.69, 112.46, 68.95, and 67.62 ppm [Figure S4B-d]. The spectrum of dibenzo-crownether-2NO_2 [Figure S4B-e] featured the characteristic signals of the C−NO_2 and *O*-methylene carbon nuclei at 140.56 and 68.44 ppm, respectively. The ^{13}C NMR spectrum of dibenzo-drownether-2NH_2 [Figure S4B-f] featured signals at 143.5 and 69.44 ppm for the nuclei of the C−NH_2 and *O*-methylene carbon atoms.[51] These spectral data

https://dx.doi.org/10.1021/acs.macromol.9b02519
Macromolecules 2020, 53, 2420−2429

confirmed our successful synthesis of dibenzo-crownether-2NH_2 in highly purity.

Synthesis of Crown-Ether BZ. The one-pot Mannich condensation of an aromatic phenol, an aliphatic/aromatic amine, and paraformaldehyde does not always proceed well for benzoxazine preparation because of low selectivity depending on the position of the substituents. Indeed, in this study, we could not synthesize our benzoxazine monomer through the one-pot Mannich condensation presented in Scheme 1e. The reaction conditions such as reaction time and solvent effect of the crown ether-functionalized benzoxazine monomer using a one-pot Mannich condensation approach are summarized in Table S1. Ishida and Lin et al. provided another method for the synthesis of benzoxazine monomers[52−54] from *o*-hydroxybenzylamine, which is readily prepared through the reduction of a Schiff base; a ring-closing reaction of *o*-hydroxybenzylamine with an aldehyde derivative then affords the benzoxazine monomer without any complicated side reactions. As such, we prepared the precursor of our difunctional benzoxazine monomer through reduction of the Schiff base formed from dibenzo-crownether-2NH_2 and salicylaldehyde [Scheme 1f]. Subsequent reaction of the resulting *o*-hydroxybenzylamine derivative [Scheme 1g] with paraformaldehyde in 1,4-dioxane and absolute EtOH at 100 °C for 12 h provided the target crown-ether BZ [Scheme 1h].

Figure 1A displays the ^{1}H NMR spectra, recorded at room temperature, of dibenzo-crownether-salicylaldehyde, dibenzo-crownether-hydroxybenzylamine, and crown-ether BZ in DMSO-d_6. The characteristic signals for the OH group of the phenolic units and the N═CH groups of dibenzo-crownether-salicylaldehyde [Figure 1A-a] were centered at 13.34 and 8.96 ppm, respectively. The spectrum of dibenzo-crownether-hydroxybenzylamine [Figure 1A-c] featured signals at 7.12−6.03 ppm for the aromatic protons; the signal for the N═CH group at 8.96 ppm had disappeared, and a new peak for NHC**H**$_2$ group appeared at 3.94 ppm, whereas signals appeared for the protons of the NH and OH groups that were consistent with their intramolecular hydrogen bonding. The spectrum of crown-ether BZ [Figure 1A-e] featured signals at 7.08−6.55 ppm for the aromatic protons and at 5.36 (OCH_2N) and 4.56 ($ArCH_2N$) ppm, at a 1:1 ratio, for the protons of the oxazine ring. Furthermore, we recorded ^{13}C NMR spectra [Figure 1B] to confirm the chemical structures of dibenzo-crownether-salicylaldehyde, dibenzo-crownether-hydroxybenzylamine, and crown-ether BZ. The ^{13}C NMR spectrum of dibenzo-crownether-salicylaldehyde [Figure 1B-b] featured signals at 161.28, 148.52, 68.85, and 67.86 ppm for the COH, N═CH, and O−CH_2 carbon nuclei, respectively. The spectrum of dibenzo-crownether-hydroxybenzylamine [Figure 1B-d] featured characteristic signals for the carbon nuclei at 158.42−99.03 (aromatic) and 42.69 (NH−CH_2) ppm. As displayed in Figure 1B-f, the characteristic signals for the oxazine unit in crown-ether BZ appeared at 79.67 (OCH_2N) and 49.56 ($ArCH_2N$) ppm.

Figure S5 presents the FTIR spectra of dibenzo[18]crown-6, dibenzo-crownether-2NO_2, dibenzo-crownether-2NH_2, dibenzo-crownether-salicylaldehyde, dibenzo-crownether- hydroxybenzylamine, and crown-ether BZ. The spectrum of dibenzo[18]crown-6 [Figure S5a] featured absorption bands for aromatic C−H stretching, aliphatic C−H stretching, and C−O−C stretching at 3051, 2922, and 1255 cm^{-1}, respectively. The spectrum of dibenzo-crownether-2NO_2 [Figure S5b] featured absorption bands at 3083, 1517, and 1347 cm^{-1} for stretching of the aromatic C−H and NO_2 groups. Signals appeared at 3428 and 3356 cm^{-1} for N−H stretching in dibenzo-crownether-2NH_2 [Figure S5c]. The typical absorption bands of dibenzo-crownether-salicylaldehyde [Figure S5d] were centered at 831, 1599, 1619, 3064, 1620, and 3446 cm^{-1}, corresponding to stretching of the aromatic rings, C═N bonds, and the O−H groups of the phenolic units. The spectrum of dibenzo-crownether-hydroxybenzylamine [Figure S5e] featured absorption bands at 3383 and 2940 cm^{-1} for N−H and aliphatic C−H stretching. The FTIR spectrum of crown-ether BZ [Figure S5f] featured absorption bands at 1360, 1240, 1044, and 937 cm^{-1} representing vibrations of its tetrasubstituted benzene ring, asymmetric C−O−C stretching, symmetric C−O−C stretching, and the oxazine ring. The purity of crown-ether BZ was confirmed using high-resolution mass spectrometry; the signal that appeared for the [M + Na]$^+$ ion was consistent with the molecular weight predicted for crown-ether BZ (Figure S6). Thus, FTIR spectroscopy, NMR spectroscopy, and high-resolution mass spectrometry confirmed our successful preparation of crown-ether BZ with high purity.

Thermal Curing Polymerization of Crown Ether-Functionalized Benzoxazine Monomer. The DSC thermogram of pure crown-ether BZ [Figure 2A] revealed two

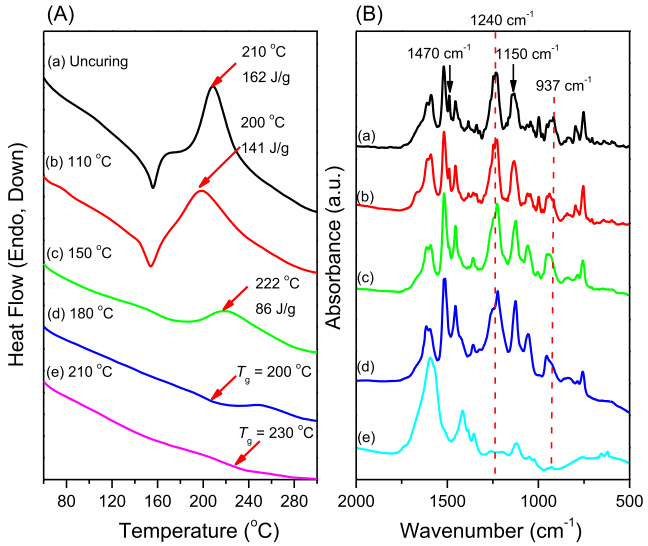

Figure 2. (A) DSC and (B) FTIR spectral analyses of crown-ether BZ at various temperatures: (a) uncured; (b) 110, (c) 150, (d) 180, and (e) 210 °C.

thermal events. The first was an endothermic process centered at 152 °C, attributed to the melting temperature of the benzoxazine monomer. The second thermal process was exothermic with a curing temperature of 210 °C and a heat of polymerization of 162 J g^{-1}. The sharpness of these endothermic and exothermic peaks confirmed the high purity of crown-ether BZ. According to the DSC thermogram, the polymerization exotherm maximum temperature for crown-ether BZ (210 °C) was significantly lower than that of the typical benzoxazine monomer 3-phenyl-3,4-dihydro-2*H*-benzooxazine (Pa, 255−263 °C),[55,56] presumably because the flexibility of the crown ether moiety on the main chain backbone structure catalyzed the ring opening polymerization at a relatively lower temperature. As displayed in Figure 2A, after the first polymerization step at 110 °C, the endothermic

https://dx.doi.org/10.1021/acs.macromol.9b02519
Macromolecules 2020, 53, 2420−2429

Scheme 2. Thermal Curing Structures of (a,b) Pure Crown-ether BZ and (c,d) Crown-ether BZ/$LiClO_4$ Complex (a,c) before and (b,d) after Thermal Curing

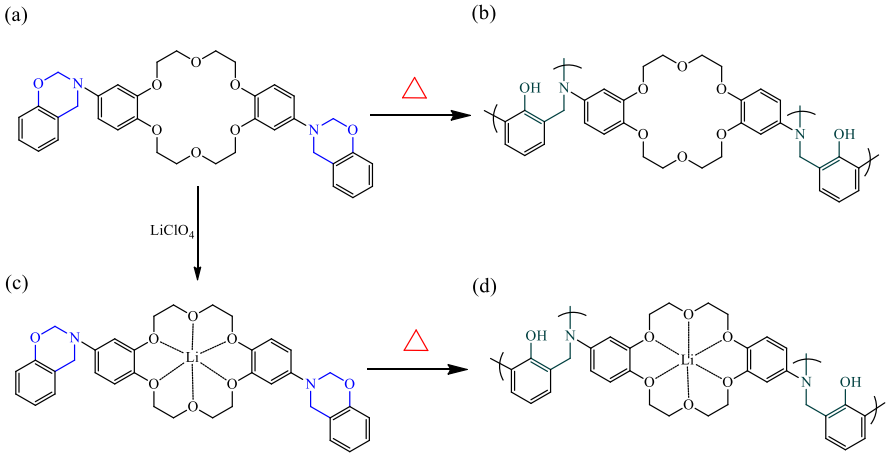

peak of crown-ether BZ remained, and the maximum exothermic curing temperature was shifted to 200 °C with a decrease in the reaction heat of 160 J g^{-1}. Furthermore, the polymerization temperature of crown-ether BZ shifted to 222 °C with a reaction heat of 86 J g^{-1} after thermal treatment at 150 °C. After thermal treatment of crown-ether BZ at 180 °C for 2 h, the intensity of the exothermic curing peak decreased and a glass transition temperature (T_g) appeared at 200 °C. Furthermore, after thermal treatment at 210 °C for 2 h, we observed no thermal events, indicating that complete ring opening polymerization of the benzoxazine monomer had occurred at this temperature; the value of T_g was 230 °C. In addition, we also check DMA analysis of crown-ether BZ after thermal curing at 210 °C for 2 h as displayed in Figure S7, indicating that the main T_g value was observed at 264 °C, which is higher than DSC analysis. This result is reasonable as the T_g value from DMA analysis is generally higher than that of DSC analysis. Notably, our new crown-ether BZ monomer was readily transformed into better processing-friendly state without the need for any catalyst and the prepolymer was obtained after a second round of thermal treatment at 150 °C.[57] We used qualitative in situ FTIR spectroscopy to investigate the ring opening polymerization of crown-ether BZ [Figure 2B]. We monitored the disappearance of the characteristic absorption bands at 1240 and 937 cm^{-1} to examine the ring opening polymerization of the oxazine ring of crown-ether BZ. For the pure crown-ether BZ and after thermal treatment at 110 °C, we found that the typical absorption bands of the oxazine ring remained at 1360, 1240, 1044, and 937 cm^{-1}, representing the vibrations of the tetrasubstituted benzene ring, asymmetric C−O−C stretching, symmetric C−O−C stretching, and oxazine ring, respectively. After thermal curing at temperatures from 150 to 180 °C, the intensities of the signals decreased for the asymmetric C−O−C and oxazine ring. The polymerization of crown-ether BZ at 210 °C led to complete disappearance of the oxazine absorption bands and confirmed the complete ring opening polymerization of the benzoxazine monomer and the formation of a highly cross-linked poly(crown-ether BZ) [Scheme 2b], consistent with the DSC analyses in Figure 2A. To further understand the effect of crown-ether BZ on the thermal ring opening polymerization, the copolymerization of the crown-ether BZ with Pa type BZ was also investigated as shown in Figure S8. We found that the exothermic curing temperature of crown-ether BZ/Pa-type (50/50) was centered at 226 °C with a heat reaction of 294 J g^{-1}, which is between pure Pa and crown ether BZ as would be expected.

We used TGA to investigate the thermal stability of crown-ether BZ and poly(crown-ether BZ) after thermal treatment at various temperatures. Figure 3 reveals that the thermal

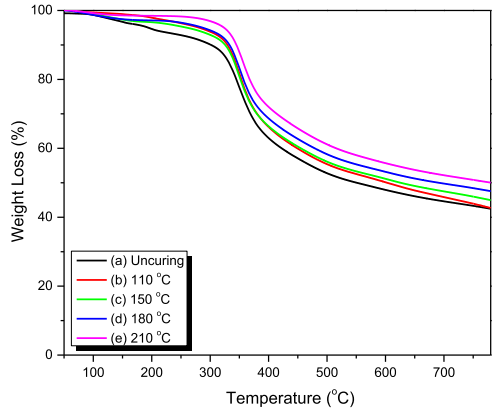

Figure 3. TGA profiles of crown-ether BZ at various temperatures: (a) uncured; (b) 110, (c) 150, (d) 180, and (e) 210 °C under a N_2 atmosphere.

decomposition temperatures (T_{d10}) of the uncured crown-ether BZ and its thermally cured (110, 150, 180, and 210 °C) samples were 211, 319, 329, 333, and 343 °C, respectively; the corresponding char yields were 42, 43, 45, 47, and 50 wt %, respectively. Thus, the values of T_{d10} and the char yields both increased upon increasing the curing temperature, consistent with a higher cross-linking density after ring opening polymerization of the crown-ether BZ.

Characterization of Crown-ether BZ/$LiClO_4$ Complexes. Because crown ether units are excellent complexing agents for capturing metal cations within their cavities, we tested the ability of our materials to bind Li^+ ions, as a model metal cation. Lithium ions readily form Li^+/crown ether complexes, with changes in the corresponding ionic conductivity, allowing ready investigations into the formation of Li^+/crown ether complexes. Initially, we used DSC to examine the thermal ring opening polymerization behavior of crown-ether BZ/$LiClO_4$ complexes. Figure 4 reveals that the thermal

https://dx.doi.org/10.1021/acs.macromol.9b02519
Macromolecules 2020, 53, 2420−2429

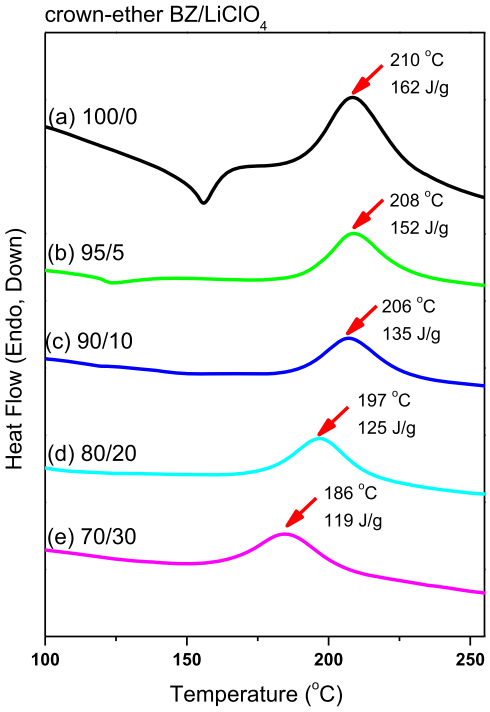

Figure 4. DSC thermograms of crown-ether BZ/$LiClO_4$ complexes prepared at weight ratios of (a) 100/0, (b) 95/5, (c) 90/10, (d) 80/20, and (e) 70/30, recorded prior to thermal curing treatment.

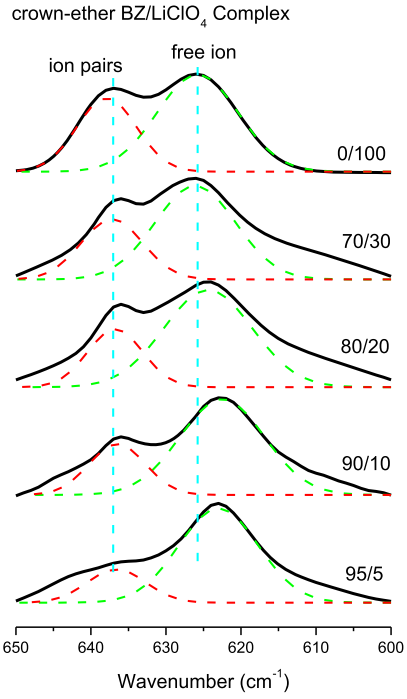

Figure 5. FTIR spectral profiles of pure $LiClO_4$ and various crown-ether BZ/$LiClO_4$ complexes, recorded at room temperature.

Table 1. Results of Curve Fitting of the Area Fraction of Free ClO_4^{-1} and Ion−Dipole Interaction between the Li^+ Cation and the ClO_4^- Anion

	free ClO_4^{-1}			ion−dipole interaction		
crown-ether BZ/$LiCLO_4$	ν, cm^{-1}	$W_{1/2}$, cm^{-1}	Af, %	ν, cm^{-1}	$W_{1/2}$, cm^{-1}	Ai, %
0/100	625.8	13	64.3	637.9	9	35.7
70/30	626.0	13	67.1	637.2	9	32.9
80/20	624.4	14	74.4	636.8	9	25.6
90/10	622.5	13	74.5	636.5	9	25.5
95/5	622.9	13	79.4	636.5	9	20.6

polymerization temperature and the reaction heat of crown-ether BZ both decreased upon increasing the $LiClO_4$ content. For example, the thermal polymerization peak temperature decreased from 210 °C for the pure crown-ether BZ to 208, 206, 197, and 186 °C when the $LiClO_4$ contents were 5, 10, 20, and 30 wt %, respectively, suggesting that the Li^+ ions acted as catalysts that facilitated ring opening polymerization of the oxazine units. Many metal ions, including Li^+, Zn^{2+}, and Fe^{3+}, are known to act as effective catalysts to accelerate the ring opening polymerizations of other benzoxazine monomers. The mechanism of metal ion-catalyzed ring opening polymerization of benzoxazine monomers proceeds in three steps: coordination of the metal ion to the oxazine ring, electrophilic attack of the metal ion to the oxazine ring, and rearrangement to give phenolic and phenoxy structures.[56,58]

We used FTIR spectroscopic analysis to gain insight into the specific metal ion/crown ether interactions of crown-ether BZ blended with various contents of $LiClO_4$ at ambient temperature (Figure 5). The FTIR spectrum of pure $LiClO_4$ [Figure 5] features two characteristic absorption bands at 626 and 637 cm^{-1}, representing the free ClO_4^- anion and the ion−dipole interaction between the Li^+ cation and the ClO_4^- anion.[59] These absorption bands of pure $LiClO_4$ shifted to 623 and 636 cm^{-1} in the presence of crown-ether BZ; these changes in wavenumber indicate that ion−dipole interactions existed between crown-ether BZ and the Li^+ cation, involving the crown ether and oxazine units. In addition, the bands for the free ClO_4^- anion and the ion pairs of the crown-ether BZ/$LiClO_4$ complexes could be deconstructed into two Gaussian peaks, as displayed in Figure 5. Table 1 summarizes the curve fitting data; the fraction of free ions increased upon increasing the concentration of crown-ether BZ. Thus, the Li^+ ions coordinated effectively to the crown ether moieties, as displayed in Scheme 2c, and the O and/or N atoms during the ring opening of the crown-ether BZ monomer.

Because Li^+ ions can act as catalysts to enhance the ring opening polymerization of oxazine units, we examined the curing kinetics of our system. Appropriate kinetic equations can help to predict and identify the thermal curing behavior of various systems involving fillers, catalysts, and additives. Figure 6 presents DSC thermograms of the pure crown-ether BZ [Figure 6A] and its complex with 20 wt % of $LiCLO_4$ [Figure 6B], recorded at various heating rates. The curing temperature (T_p) shifted to a higher temperature upon increasing the heating rate from 5 to 20 °C min^{-1}, as expected for a delay in the curing reaction. The Kissinger method is used widely to investigate the curing kinetics of the benzoxazine system; it depends on the linear relationship between the logarithm of (β/T_p^2) and the reciprocal of the peak temperature T_p. The activation energy (E_a) can be calculated according to eq 1[60]

$$\ln\left(\frac{\beta}{T_p^2}\right) = \ln\left(\frac{AR}{E_a}\right) - \frac{E_a}{RT} \quad (1)$$

https://dx.doi.org/10.1021/acs.macromol.9b02519
Macromolecules 2020, 53, 2420−2429

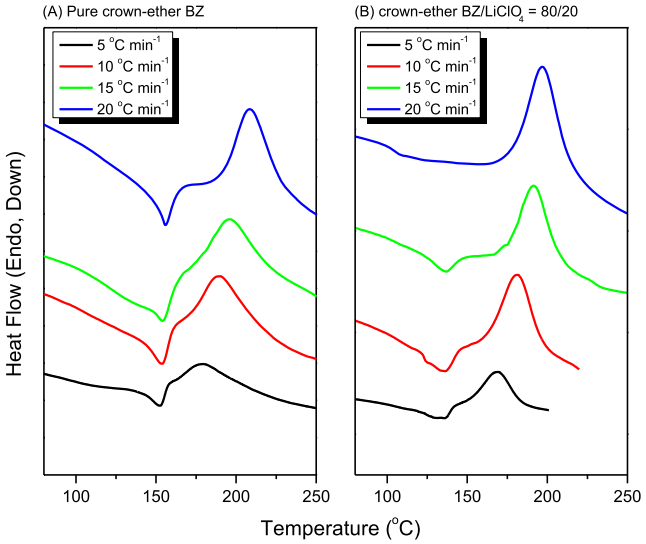

Figure 6. Dynamic DSC exothermic curves, recorded at various heating rates, for (A) pure crown-ether BZ and the (B) crown-ether BZ/$LiClO_4$ = 80/20 complex.

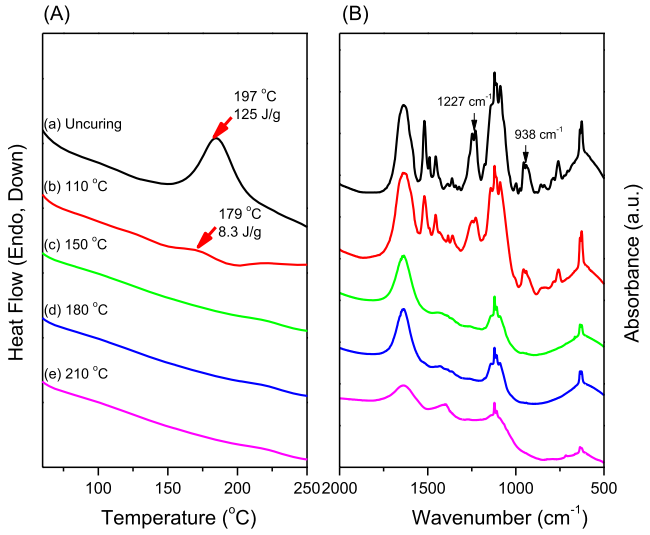

Figure 7. (A) DSC and (B) FTIR spectral analyses of the crown-ether BZ//$LiClO_4$ = 80/20 complex at various temperatures: (a) uncured; (b) 110, (c) 150, (d) 180, and (e) 210 °C.

where β, equal to dT/dt, is the heating rate; A is the pre-exponential factor; T_p is the exothermic curing peak; and R is the universal gas constant.

Figure S9 presents the plot based on eq 1; it provides the value of E_a from the slope of the line, without any assumption about the conversion-dependent function. The calculated activation energies for the pure crown-ether BZ and for its complex with 20 wt % $LiClO_4$ were 77.82 and 74.91 kJ mol^{-1}, respectively, suggesting that the presence of the crown ether moiety in the main chain backbone structure catalyzed the ring opening polymerization at relatively lower temperatures. In addition, the Li^+ ions could also act as a catalyst to enhance the ring opening polymerization of the oxazine units, because the activation energy was lower than that of the pure crown-ether BZ system.

To further examine the thermal polymerization behavior after the addition of $LiClO_4$ to the crown-ether BZ system, we used DSC and FTIR spectroscopy to evaluate the corresponding thermal curing behavior of the crown-ether BZ/$LiClO_4$ = 80/20 complex (Figure 7). The thermal curing peak of the uncured crown-ether BZ/$LiClO_4$ = 80/20 complex was located at 197 °C with a heat reaction of 125 J g^{-1} [Figure 7A]. More interestingly, a phenomenon occurred similar to that of the pure crown-ether BZ, with the maximum exothermic peak and the enthalpy of the crown-ether BZ/$LiClO_4$ = 80/20 complex, both decreasing after thermal treatment at 110 °C, and completely disappearing upon increasing the curing temperature from 150 to 210 °C; again, these features suggest that the presence of Li^+ ions assisted the ring opening process. Furthermore, Figure 7B presents corresponding FTIR spectra recorded after thermal curing of the crown-ether BZ/$LiClO_4$ = 80/20 complex at various temperatures. The characteristic absorption bands of the oxazine units at 1227 and 927 cm^{-1} disappeared after thermal curing at 150 °C, consistent with the DSC data, confirming complete ring opening polymerization of the benzoxazine monomer and the formation of a highly cross-linked poly(crown-ether BZ) in the presence of Li^+ ions, as displayed in Scheme 2d.

Ionic Conductivity of Crown-Ether BZ/$LiClO_4$ Complexes. Figure 7B also reveals significant changes in the signals for the ClO_4^- ions at 626 and 637 cm^{-1}, as summarized in Figure 8A, corresponding to the free ClO_4^- anions and the

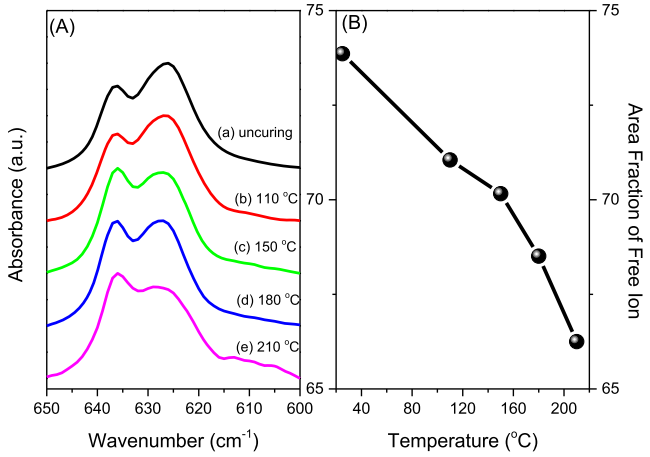

Figure 8. (A) FTIR spectral analyses of the crown-ether BZ//$LiClO_4$ = 80/20 complex at various temperatures: (a) uncured; (b) 110, (c) 150, (d) 180, and (e) 210 °C. (B) Area fractions of free ClO_4^- ions for the crown-ether BZ//$LiClO_4$ = 80/20 complex at various temperatures.

ion−dipole interaction between the Li^+ cations and ClO_4^- anions, as mentioned in Figure 5. The area fraction of the signal for the free ions near 626 cm^{-1} decreased upon increasing the thermal curing temperature [Figure 8A]; the curve fitting data, based on the deconstruction into Gaussian peaks, are summarized in Figure 8B. In general, the fraction of free ClO_4^- ions increases upon increasing the temperature because the chain mobility of the polymeric matrix increases accordingly.[59] We found, however, that the chain mobility of crown-ether BZ decreased upon increasing the temperature, because the cross-linking density of poly(crown-ether BZ) would increase. To the best of our knowledge, we are the first to observe such a decrease in the free ClO_4^- ion concentration; we suspected that the ionic conductivity of the crown-ether BZ/$LiClO_4$ complexes should also change upon increasing the temperature.

https://dx.doi.org/10.1021/acs.macromol.9b02519
Macromolecules 2020, 53, 2420−2429

Figure 9 presents the measured ionic conductivities of the crown-ether BZ/$LiClO_4$ complexes, confirming changes in

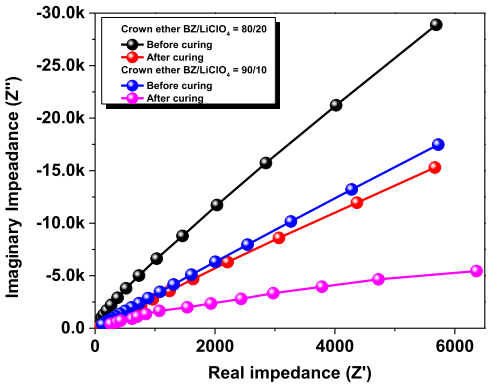

Figure 9. Electrochemical impedance spectra (Nyquist plot) of the crown-ether BZ/$LiClO_4$ = 90/10 and 80/20 complexes, recorded before and after thermal polymerization.

chain mobility at various temperatures. The ionic conductivity is known to follow the equation

$$\sigma = n \times z \times \mu \quad (2)$$

where n is the content of charge carriers, z is the ionic charge, and μ is the ionic mobility.[61−63] The electrochemical impedance spectra reveal a well-designed Warburg diffusion (W_d) combined with solution (R_s) and charge-transfer (R_{ct}) resistances matching those of a Randles cell. The values of the impedance reached 6.1×10^{-4} and 3.8×10^{-5} S cm^{-1} for the crown-ether BZ/$LiClO_4$ = 80/20 complex before (25 °C) and after thermal curing at 210 °C, respectively. In addition, the ionic conductivities reached 1.1×10^{-4} and 8.3×10^{-5} S cm^{-1} for the crown-ether BZ/$LiClO_4$ = 90/10 complex before and after thermal polymerization, respectively. These values are consistent with the Li^+ ions present within the crown ether and benzoxazine structures yielding greater conductivity. Increasing the concentration of Li^+ ions at room temperature could also enhance the ionic conductivity [cf. the values obtained at 10 and 20 wt % $LiClO_4$], because of the increase in the number of charge carrier (n). In contrast, the conductivity decreased after thermal curing for both of these crown-ether BZ/$LiClO_4$ complexes, because the chain or ionic mobility (μ) was restricted after thermal curing of crown-ether BZ, causing the Li^+ ions to transform back to $LiClO_4$ and, thereby, decrease the fraction of free ClO_4^- ions. Notably, the conductivity of 8.3×10^{-5} S cm^{-1} for the crown-ether BZ/$LiClO_4$ = 90/10 complex after thermal curing is higher than those of typical polymer-based electrolytes [e.g., PEO/$LiClO_4$ = 75/25 (3.2×10^{-7} S cm^{-1}),[62,63] PCL/$LiClO_4$ = 75/25 (4.1×10^{-8} S cm^{-1}),[62,63] PMMA/$LiClO_4$ = 80/20 (5.1×10^{-8} S cm^{-1}),[64] and PVP/$LiClO_4$ = 80/20 (4.9×10^{-9} S cm^{-1}).[64] The higher conductivity measured from the crown-ether BZ/$LiClO_4$ complexes presumably arose from the strong metal−ligand interaction from Li^+ ions with the crown ether units,[64,65] as compared with the weak interactions of Li^+ ions with the C−O−C units of PEO and with the C═O groups of PCL, PMMA, and PVP; the stronger interactions would be expected to enhance the value of the ionic charge (z). In addition, blending with different metal ions such as K^+, Zn^{+2}, or Fe^{+3} into our crown-ether BZ by a different size of metal ion is also received interesting. Figure S10 displays the DSC measurement of crown-ether BZ/$KClO_4$ = 90/10 and 80/20, respectively. We found that the exothermic curing peak of crown-ether BZ was shifted to a higher temperature, indicating that Li^+ is a very good catalyst for ring-opening polymerization for a oxazine unit compared to K^+. In addition, the Li^+ ion possesses the ability to migrate faster through the electrolyte medium because of the high rate of diffusion and small size of the ion compared to other larger cations such as K^+, Rb^+, and Cs^+. These larger cations would possess less of the affinity for the oxygen atoms for crown ether electrolytes. More importantly, thermal curing of the crown-ether BZ/$LiClO_4$ complexes would enhance their thermal and mechanical properties relative to those of typical thermoplastic resins, a potentially useful feature for the next generation of polymer solid electrolytes.

CONCLUSIONS

We have prepared a new crown ether-functionalized benzoxazine monomer through reduction of the Schiff base formed from dibenzo-crownether-2NH_2 and salicylaldehyde. NMR and FTIR spectroscopy and high-resolution mass spectrometry confirmed its chemical structure. After thermal treatment under N_2 atmosphere, the resultant poly(crown-ether BZ) exhibited excellent thermal stability and a high char yield. The exothermic curing peak of crown-ether BZ decreased significantly, to 186 °C, after the addition of 30 wt % $LiClO_4$, indicating that the flexible crown ether moieties and the Li^+ ions acted as effective catalysts and promoters that accelerated the ring opening polymerization of the benzoxazine monomer. The highest ionic conductivity (8.27×10^{-5} S cm^{-1}) was that for the crown-ether BZ/$LiClO_4$ = 90/10 complex after thermal curing; this ionic conductivity is higher than those of typical polymer-based systems, with our polymer electrolyte also displaying higher thermal and mechanical stability.

ASSOCIATED CONTENT

Supporting Information

The Supporting Information is available free of charge at https://pubs.acs.org/doi/10.1021/acs.macromol.9b02519.

DSC, mass spectroscopy, and NMR and FTIR analyses of crown-ether derivatives (PDF)

AUTHOR INFORMATION

Corresponding Author

Shiao-Wei Kuo − *Department of Materials and Optoelectronic Science, Center of Crystal Research, National Sun Yat-Sen University, Kaohsiung 80424, Taiwan; Department of Medicinal and Applied Chemistry, Kaohsiung Medical University, Kaohsiung 807, Taiwan;* orcid.org/0000-0002-4306-7171; Phone: 886-7-5254099; Email: kuosw@faculty.nsysu.edu.tw

Author

Mohamed Gamal Mohamed − *Department of Materials and Optoelectronic Science, Center of Crystal Research, National Sun Yat-Sen University, Kaohsiung 80424, Taiwan;* orcid.org/0000-0003-0301-8372

Complete contact information is available at: https://pubs.acs.org/10.1021/acs.macromol.9b02519

https://dx.doi.org/10.1021/acs.macromol.9b02519
Macromolecules 2020, 53, 2420−2429

Notes

The authors declare no competing financial interest.

■ ACKNOWLEDGMENTS

This study was supported financially by the Ministry of Science and Technology, Taiwan, under contracts MOST 106-2221-E-110- 067-MY3, 108-2638-E-002-003-MY2, and 108-2221-E-110 -014-MY3. We thank Dr. Mahmoud M. M. Ahmed at the National Sun Yat-Sen University for Ionic Conductivity Measurement.

■ REFERENCES

(1) Zhang, K.; Liu, Y.; Ishida, H. Polymerization of an AB-Type Benzoxazine Monomer toward Different Polybenzoxazine Networks: When Diels−Alder Reaction Meets Benzoxazine Chemistry in a Single-Component Resin. *Macromolecules* **2019**, *52*, 7386−7395.

(2) Zhang, K.; Han, L.; Froimowicz, P.; Ishida, H. A smart latent catalyst containing o-trifluoroacetamide functional benzoxazine: precursor for low temperature formation of very high Performance polybenzoxazole with low dielectric constant and high thermal stability. *Macromolecules* **2017**, *50*, 6552−6560.

(3) Kiskan, B.; Yagci, Y. Thermally curable benzoxazine monomer with a photodimerizable coumarin group. *J. Polym. Sci., Part A: Polym. Chem.* **2017**, *45*, 1670−1676.

(4) El-Mahdy, A. F. M.; Kuo, S.-W. Direct synthesis of poly(benzoxazine imide) from an ortho-benzoxazine: its thermal conversion to highly cross-linked polybenzoxazole and blending with poly(4-vinylphenol). *Polym. Chem.* **2018**, *9*, 1815−1826.

(5) Wu, J.; Xi, Y.; Mccandless, G. T.; Xie, Y.; Menon, R.; Patel, Y.; Yang, D. J.; Iacono, S. T.; Novak, B. M.; Iacono, S. T.; Novak, B. M. Synthesis and characterization of partially fluorinated polybenzoxazine resins utilizing octafluorocyclopentene as a versatile building block. *Macromolecules* **2015**, *48*, 6087−6095.

(6) Wang, C.; Sun, J.; Liu, X.; Sudo, A.; Endo, T. Synthesis and copolymerization of fully bio-based benzoxazines from guaiacol, furfurylamine and stearylamine. *Green Chem.* **2012**, *14*, 2799−2806.

(7) Mohamed, M. G.; Kuo, S. W. Functional Silica and Carbon Nanocomposites Based on Polybenzoxazines. *Macromol. Chem. Phys.* **2019**, *220*, 1800306−1800318.

(8) Mohamed, M.; Kuo, S.-W. Polybenzoxazine/Polyhedral Oligomeric Silsesquioxane (POSS) Nanocomposites. *Polymers* **2016**, *8*, 225−244.

(9) Liu, Y.; Yin, R.; Yu, X.; Zhang, K. Modification of solventless synthesized benzoxazine resin by phthalonitrile group: An effective approach for enhancing thermal stability of polybenzoxazines. *Macromol. Chem. Phys.* **2018**, *220*, 1800291−1800297.

(10) Arslan, M.; Kiskan, B.; Yagci, Y. Benzoxazine-Based Thermoset with Autonomous Self-Healing and Shape Recovery. *Macromolecules* **2018**, *51*, 10095−10103.

(11) Ghosh, N. N.; Kiskan, B.; Yagci, Y. Polybenzoxazines-New High-Performance Thermosetting Resins: Synthesis and Properties. *Prog. Polym. Sci.* **2007**, *32*, 1344−1391.

(12) Chutayothin, P.; Ishida, H. Cationic Ring-Opening Polymerization of 1,3-Benzoxazines: Mechanistic Study Using Model Compounds. *Macromolecules* **2010**, *43*, 4562−4572.

(13) Sudo, A.; Du, L.-C.; Hirayama, S.; Endo, T. Substituent Effects of N-Alkyl Groups on Thermally Induced Polymerization Behavior of 1,3-Benzoxazines. *J. Polym. Sci., Part A: Polym. Chem.* **2010**, *48*, 2777−2782.

(14) Kaya, G.; Kiskan, B.; Yagci, Y. Phenolic Naphthoxazines as Curing Promoters for Benzoxazines. *Macromolecules* **2018**, *51*, 1688−1695.

(15) Wu, J.-Y.; Mohamed, G. M.; Kuo, S.-W. Directly synthesized nitrogen-doped microporous carbons from polybenzoxazine resins for carbon dioxide capture. *Polym. Chem.* **2017**, *8*, 5481−5489.

(16) Aydogan, C.; Kiskan, B.; Hacioglu, S. O.; Toppare, L.; Yagci, Y. Electrochemical Manipulation of Adhesion Strength of Polybenzoxazines on Metal Surfaces: From Strong Adhesion to Dismantling. *RSC Adv.* **2014**, *4*, 27545−27551.

(17) Laobuthee, A.; Chirachanchai, S.; Ishida, H.; Tashiro, K. Asymmetric Mono-oxazine: An Inevitable Product from Mannich Reaction of Benzoxazine Dimers. *J. Am. Chem. Soc.* **2001**, *123*, 9947−9955.

(18) Rungswang, W.; Kotaki, M.; Shimojima, T.; Kimura, G.; Sakurai, S.; Chirachanchai, S. Directing Thermoplastic Elastomer Microdomain Parallel to Fiber Axis: A Model Case of SEBS with Benzoxazine through π-π Stacking. *Macromolecules* **2011**, *44*, 9276−9285.

(19) Lin, C. H.; Chang, S. L.; Shen, T. Y.; Shih, Y. S.; Lin, H. T.; Wang, C. F. Flexible Polybenzoxazine Thermosets with High Glass Transition Temperatures and Low Surface Free Energies. *Polym. Chem.* **2012**, *3*, 935−945.

(20) Taskin, O. S.; Kiskan, B.; Aksu, A.; Balkis, N.; Weber, J.; Yagci, Y. Polybenzoxazine: A Powerful Tool for Removal of Mercury Salts from Water. *Chem.—Eur. J.* **2014**, *20*, 10953−10958.

(21) Laobuthee, A.; Chirachanchai, S. A Simple, Effective, and Selective Synthesis Route for Difunctional 30-Membered Macrocyclic Ester and Linear Oligoester Derived from Benzoxazine Dimers. *Chem. Lett.* **2002**, *31*, 614−615.

(22) Wang, M. W.; Jeng, R. J.; Lin, C. H. Study on the Ring-Opening Polymerization of Benzoxazine through Multisubstituted Polybenzoxazine Precursors. *Macromolecules* **2015**, *48*, 530−535.

(23) Zhao, J.; Gilani, M. R. H. S.; Lai, J.; Nsabimana, A.; Liu, Z.; Luque, R.; Xu, G. Autocatalysis Synthesis of Poly(benzoxazine-co-resol)-Based Polymer and Carbon Spheres. *Macromolecules* **2018**, *51*, 5494−5500.

(24) Wang, C.-F.; Su, Y.-C.; Kuo, S.-W.; Huang, C.-F.; Sheen, Y.-C.; Chang, F.-C. Low-Surface-Free-Energy Materials Based on Polybenzoxazines. *Angew. Chem., Int. Ed.* **2006**, *45*, 2248−2251.

(25) Ishida, H. *Handbook of Polybenzoxazine Resins*; Ishida, H., Agag, T., Eds.; Elsevier: Amsterdam, 2011.

(26) Sawaryn, C.; Landfester, K.; Taden, A. Benzoxazine miniemulsions stabilized with polymerizable nonionic benzoxazine surfactants. *Macromolecules* **2010**, *43*, 8933−8941.

(27) Huang, J.-M.; Kuo, S.-W.; Lee, Y.-J.; Chang, F.-C. Synthesis and Characterization of a Vinyl-Terminated Benzoxazine Monomer and its Blends with Poly(ethylene oxide). *J. Polym. Sci., Part B: Polym. Phys.* **2007**, *45*, 644−653.

(28) Demir, K. D.; Kiskan, B.; Yagci, Y. Thermally Curable Acetylene-Containing Main-Chain Benzoxazine Polymers via Sonogashira Coupling Reaction. *Macromolecules* **2011**, *44*, 1801−1807.

(29) Zhang, K.; Yu, X. Catalyst-Free and Low-Temperature Terpolymerization in a Single-Component Benzoxazine Resin Containing Both Norbornene and Acetylene Functionalities. *Macromolecules* **2018**, *51*, 6524−6533.

(30) Kudoh, R.; Sudo, A.; Endo, T. A Highly Reactive Benzoxazine Monomer, 1-(2-Hydroxyethyl)-1,3-Benzoxazine: Activation of Benzoxazine by Neighboring Group Participation of Hydroxyl Group. *Macromolecules* **2010**, *43*, 1185−1187.

(31) Ye, Y. S.; Huang, Y. J.; Chang, F. C.; Xue, Z. G.; Xie, X. L. Synthesis and characterization of thermally cured polytriazole polymers incorporating main or side chain benzoxazine crosslinking moieties. *Polym. Chem.* **2014**, *5*, 2863−2871.

(32) Schäfer, H.; Koschek, K. Effect of poly(ϵ-caprolactone) in polybenzoxazine blends and respective copolymers on morphology and mechanical properties. *Eur. Polym. J.* **2018**, *108*, 582−590.

(33) Sawaryn, C.; Kreiling, S.; Schönfeld, R.; Landfester, K.; Taden, A. *Benzoxazines for Industrial Applications Comparison with Other Resins, Formulation and Toughening Know-How, and Water-Based Dispersion Technology*; Ishida, H., Agag, T., Eds.; Elsevier: Amsterdam, 2011; Chapter 35, pp 605−620.

(34) Schäfer, H.; Hartwig, A.; Koschek, K. The nature of bonding matters: Benzoxazine based shape memory polymers. *Polymer* **2018**, *135*, 285−294.

(35) Brown, E. A.; Rider, D. A. Pegylated Polybenzoxazine Networks with Increased Thermal Stability from Miscible Blends of Tosylated

https://dx.doi.org/10.1021/acs.macromol.9b02519
Macromolecules 2020, 53, 2420−2429

Poly(ethylene glycol) and a Benzoxazine Monomer. *Macromolecules* **2017**, *50*, 6468−6481.
(36) Ohashi, S.; Iguchi, D.; Heyl, T. R.; Froimowicz, P.; Ishida, H. Quantitative studies on the p-substituent effect of the phenolic component on the polymerization of benzoxazines. *Polym. Chem.* **2018**, *9*, 4194−4204.
(37) Mohamed, M. G.; Hsiao, C.-H.; Luo, F.; Dai, L.; Kuo, S.-W. Multifunctional polybenzoxazine nanocomposites containing photo-responsive azobenzene units, catalytic carboxylic acid groups, and pyrene units capable of dispersing carbon nanotubes. *RSC Adv.* **2015**, *5*, 45201−45212.
(38) Shih, H.-K.; Hsieh, C.-C.; Mohamed, M. G.; Zhu, C.-Y.; Kuo, S.-W. Ternary polybenzoxazine/POSS/SWCNT hybrid nanocomposites stabilized through supramolecular interactions. *Soft Matter* **2016**, *12*, 1847−1858.
(39) Araz, C. R.; Ishida, H.; Maurer, F. H. Quantifying Dispersion in Graphene Oxide/Reactive Benzoxazine Monomer Nanocomposites. *Macromolecules* **2014**, *47*, 3685−3692.
(40) Zeng, M.; Wang, J.; Li, R.; Liu, J.; Chen, W.; Xu, Q.; Gu, Y. The curing behavior and thermal property of graphene oxide/benzoxazine nanocomposites. *Polymer* **2013**, *54*, 3017−3116.
(41) Fu, H.-K.; Huang, C.-F.; Kuo, S.-W.; Lin, H.-C.; Yei, D.-R.; Chang, F.-C. Effect of an Organically Modified Nanoclay on Low-Surface-Energy Materials of Polybenzoxazine. *Macromol. Rapid Commun.* **2008**, *29*, 1216−1220.
(42) Zhang, K.; Zhuang, Q.; Liu, X.; Yang, G.; Cai, R.; Han, Z. A New Benzoxazine Containing Benzoxazole-Functionalized Polyhedral Oligomeric Silsesquioxane and the Corresponding Polybenzoxazine Nanocomposites. *Macromolecules* **2013**, *46*, 2696−2704.
(43) Kirschbaum, S.; Landfester, K.; Taden, A. Synthesis and Thermal Curing of Benzoxazine Functionalized Polyurethanes. *Macromolecules* **2015**, *48*, 3811−3816.
(44) Liao, Y.-T.; Lin, Y.-C.; Kuo, S.-W. Highly Thermally Stable, Transparent, and Flexible Polybenzoxazine Nanocomposites by Combination of Double-Decker-Shaped Polyhedral Silsesquioxanes and Polydimethylsiloxane. *Macromolecules* **2017**, *50*, 5739−5747.
(45) Chen, W.-C.; Kuo, S.-W. Ortho-Imide and Allyl Groups Effect on Highly Thermally Stable Polybenzoxazine/Double-Decker-Shaped Polyhedral Silsesquioxane Hybrids. *Macromolecules* **2018**, *51*, 9602−9612.
(46) Marczenko, K. M.; Mercier, H. P. A.; Schrobilgen, G. J. A Stable Crown Ether Complex with a Noble-Gas Compound. *Angew. Chem., Int. Ed.* **2018**, *57*, 12448−12452.
(47) Bond, A. H.; Dietz, M. L.; Chiarizia, R. Incorporating Size Selectivity into Synergistic Solvent Extraction: A Review of Crown Ether-Containing Systems. *Ind. Eng. Chem. Res.* **2000**, *39*, 3442−3464.
(48) Zheng, B.; Wang, F.; Dong, S.; Huang, F. Supramolecular polymers constructed by crown ether-based molecular recognition. *Chem. Soc. Rev.* **2012**, *41*, 1621−1636.
(49) Huang, D.; Zhang, Q.; Deng, Y.; Luo, Z.; Li, B.; Shen, X.; Qi, Z.; Dong, S.; Ge, Y.; Chen, W. Polymeric crown ethers: LCST behavior in water and stimuli-responsiveness. *Polym. Chem.* **2018**, *9*, 2547−2579.
(50) Kazemabad, M.; Verliefde, A.; Cornelissen, E. R.; D'Haese, A. Crown ether containing polyelectrolyte multilayer membranes for lithium recovery. *J. Membr. Sci.* **2020**, *595*, 117432.
(51) Patel, H. A.; Selberg, J.; Salah, D.; Chen, H.; Liao, Y.; Mohan Nalluri, S. K.; Farha, O. K.; Snurr, R. Q.; Rolandi, M.; Stoddart, J. F. Proton Conduction in Tröger's Base-Linked Poly(crown ether)s. *ACS Appl. Mater. Interfaces* **2018**, *10*, 25303−25310.
(52) Lin, C. H.; Chang, S. L.; Hsieh, C. W.; Lee, H. H. Aromatic diamine-based benzoxazines and their high-performance thermosets. *Polymer* **2008**, *49*, 1220−1229.
(53) Ohashi, S.; Pandey, V.; Arza, C. R.; Froimowicz, P.; Ishida, H. Simple and low energy consuming synthesis of cyanate ester functional naphthoxazines and their properties. *Polym. Chem.* **2016**, *7*, 2245−2252.
(54) Ohashi, S.; Cassidy, F.; Huang, S.; Chiou, K.; Ishida, H. Synthesis and ring-opening polymerization of 2-substituted 1,3-benzoxazine: the first observation of the polymerization of oxazine ring-substituted benzoxazines. *Polym. Chem.* **2016**, *7*, 7177−7184.
(55) Mohamed, M. G.; Lin, R.-C.; Tu, J.-H.; Lu, F.-H.; Hong, J.-L.; Jeong, K.-U.; Wang, C.-F.; Kuo, S.-W. Thermal Property and Aggregation-Induced Emission Fluorophore That Forms Metal-Ligand Complexes with $Zn(ClO_4)_2$ of Salicylaldehyde Azine-Functionalized Polybenzoxazine. *RSC Adv.* **2015**, *5*, 65635−65645.
(56) Mohamed, M. G.; Su, W.-C.; Lin, Y.-C.; Wang, C.-F.; Chen, J.-K.; Jeong, K.-U.; Kuo, S.-W. Azopyridine-functionalized benzoxazine with $Zn(ClO_4)_2$ form high-performance polybenzoxazine stabilized through metal-ligand coordination. *RSC Adv.* **2014**, *4*, 50373−50385.
(57) Salum, M. L.; Iguchi, D.; Arza, C. R.; Han, L.; Ishida, H.; Froimowicz, P. Making Benzoxazines Greener: Design, Synthesis, and Polymerization of a Biobased Benzoxazine Fulfilling Two Principles of Green Chemistry. *ACS Sustainable Chem. Eng.* **2018**, *6*, 13096−13106.
(58) Liu, C.; Shen, D.; Sebastián, R. M.; Marquet, J.; Schönfeld, R.; Schönfeld, R. Mechanistic Studies on Ring-Opening Polymerization of Benzoxazines: A Mechanistically Based Catalyst Design. *Macromolecules* **2011**, *44*, 4616−4622.
(59) Kuo, S.-W.; Huang, C.-F.; Wu, C.-H.; Chang, F.-C. Thermal and Spectroscopic Properties of Zinc Perchlorate/Poly (vinylpyrrolidone) Blends and a Comparison with Related Hydrogen Bonding Systems. *Polymer* **2004**, *45*, 6613−6621.
(60) Kissinger, H. E. Reaction Kinetics in Differential Thermal Analysis. *Anal. Chem.* **1957**, *29*, 1702−1706.
(61) Chiu, C.-Y.; Chen, H.-W.; Kuo, S.-W.; Huang, C.-F.; Chang, F.-C. Investigating the Effect of Miscibility on the Ionic Conductivity of LiClO4/PEO/PCL Ternary Blends. *Macromolecules* **2004**, *37*, 8424−8430.
(62) Chiu, C.-Y.; Hsu, W.-H.; Yen, Y.-J.; Kuo, S.-W.; Chang, F.-C. Miscibility Behavior and Interaction Mechanism of Polymer Electrolytes Comprising $LiClO_4$ and MPEG-block-PCL Copolymers. *Macromolecules* **2005**, *38*, 6640−6647.
(63) Chiu, C.-Y.; Yen, Y.-J.; Kuo, S.-W.; Chen, H.-W.; Chang, F.-C. Complicated Phase Behavior and Ionic Conductivities of PVP-co-PMMA-Based Polymer Electrolytes. *Polymer* **2007**, *48*, 1329−1342.
(64) Laobuthee, A.; Ishida, H.; Chirachanchai, S. Metal Ion Guest Responsive Benzoxazine Dimers and Inclusion Phenomena of Cyclic Derivatives. *J. Inclusion Phenom. Macrocyclic Chem.* **2003**, *47*, 179−185.
(65) Chirachanchai, S.; Phongtamrug, S.; Tashiro, K. *Supramolecular Chemistry of Benzoxazines: From Simple, Selective, Effective, and Efficient Macrocyclization Pathways to Host-Guest Properties*; Ishida, H., Agag, T., Eds.; Elsevier: Amsterdam, 2011; Chapter 17, pp 331−354.

https://dx.doi.org/10.1021/acs.macromol.9b02519
Macromolecules 2020, 53, 2420−2429